



**HAL**  
open science

# Carbohydrate-attached Fullerene Derivative for Selective Localization in Ordered Carbohydrate-block-Poly(3-hexylthiophene) Nanodomains

Yoko Sakai-Otsuka, Yu Ogawa, Toshifumi Satoh, Wen-Chang Chen,  
Redouane Borsali

► **To cite this version:**

Yoko Sakai-Otsuka, Yu Ogawa, Toshifumi Satoh, Wen-Chang Chen, Redouane Borsali. Carbohydrate-attached Fullerene Derivative for Selective Localization in Ordered Carbohydrate-block-Poly(3-hexylthiophene) Nanodomains. Carbohydrate Polymers, 2021, 255, pp.117528. 10.1016/j.carbpol.2020.117528 . hal-03431862

**HAL Id: hal-03431862**

**<https://hal.science/hal-03431862>**

Submitted on 16 Nov 2021

**HAL** is a multi-disciplinary open access archive for the deposit and dissemination of scientific research documents, whether they are published or not. The documents may come from teaching and research institutions in France or abroad, or from public or private research centers.

L'archive ouverte pluridisciplinaire **HAL**, est destinée au dépôt et à la diffusion de documents scientifiques de niveau recherche, publiés ou non, émanant des établissements d'enseignement et de recherche français ou étrangers, des laboratoires publics ou privés.

1 **Carbohydrate-attached Fullerene Derivative for Selective Localization in Ordered**  
2 **Carbohydrate-*block*-Poly(3-hexylthiophene) Nanodomains**

3 Yoko Sakai-Otsuka <sup>a</sup>, Yu Ogawa <sup>a</sup>, Toshifumi Satoh <sup>b</sup>, Wen-Chang Chen <sup>c</sup>,  
4 and Redouane Borsali <sup>a,\*</sup>

5  
6 <sup>a</sup> *Univ Grenoble Alpes, CNRS, CERMAV, F-38000 Grenoble, France*

7 <sup>b</sup> *Laboratory of Polymer Chemistry, Division of Applied Chemistry,*

8 *Faculty of Engineering, Hokkaido University, N13W8, Kita-ku, Sapporo, 060-8628, Japan.*

9 <sup>c</sup> *Advanced Research Center for Green Materials Science and Technology, National Taiwan*  
10 *University, Taipei 10617, Taiwan*

11  
12  
13 *\* Corresponding Author*

14 *Redouane Borsali – Univ Grenoble Alpes, CERMAV, CNRS, F-38000 Grenoble, France;*

15 *ORCID: <https://orcid.org/0000-0002-7245-586X>*

16 *Email Address: [borsali@cermav.cnrs.fr](mailto:borsali@cermav.cnrs.fr)*

17  
18 **ABSTRACT**

19 A carbohydrate-based fullerene derivative (AcMal<sub>7</sub>-C<sub>61</sub>) is designed, synthesized and applied  
20 to a lamellar-forming high- $\chi$  block copolymer system, poly(3-hexylthiophene)-*block*-  
21 peracetylated maltoheptaose (P3HT-*b*-AcMal<sub>7</sub>), to actualize an ordered donor/acceptor (D/A)  
22 network. A well-defined D/A lamellar structure of the P3HT-*b*-AcMal<sub>7</sub>:AcMal<sub>7</sub>-C<sub>61</sub> blend with  
23 sub-10 nm domain features is achieved upon thermal annealing. The AcMal<sub>7</sub>-C<sub>61</sub> molecules are  
24 localized in the phase-separated AcMal<sub>7</sub> nanodomains without causing the formation of  
25 fullerene crystals while maintaining the lamellar morphology up to 1:0.5 (D:A) blending ratio.  
26 The cross-sectional TEM observation and GISAXS measurement reveals that the P3HT-*b*-  
27 AcMal<sub>7</sub> tends to spontaneously organize into lamellar structures oriented perpendicular to the  
28 film surface at the air/film interface while the domain orientation at the bottom interface  
29 depends on the nature of the substrate.

30 *Keywords:*

31 Carbohydrate-based semiconducting block copolymers

32 Self-assembly

33 Nanostructured bulk heterojunction

34 Fullerene derivative

35 Organic photovoltaics

36

37

## 38 1. Introduction

39 Organic photovoltaics (OPVs) have been intensively studied in the past two decades in  
40 response to social demand for renewable energy technologies that can fulfill the needs for low-  
41 cost, light weight, and flexible energy devices (Dou et al., 2013). With extensive efforts on the  
42 device engineering and the material design, the power conversion efficiencies (PCEs) of single  
43 junction donor-acceptor (D/A) bulk-heterojunction (BHJ) solar cells have remarkably improved  
44 since the first demonstration of the BHJ concept in 1995 (Yu, Gao, Hummelen, Wudl, & Heeger,  
45 1995).

46 Block copolymers have received significant attention in the area of organic optoelectronics  
47 because of their ability to self-organize into thermodynamically stable periodic nanostructures  
48 (Lee & Gomez, 2015; Segalman, McCulloch, Kirmayer, & Urban, 2009). Regioregular poly(3-  
49 hexylthiophene), P3HT, is one of the most employed *p*-type semiconducting polymers in the  
50 block copolymer systems. However, strong  $\pi$ - $\pi$  interactions of the P3HT often prevents the  
51 microphase separation, eventually results in a randomly-oriented nanofibril structure  
52 (Boudouris, Frisbie, & Hillmyer, 2008; Iovu et al., 2007; Liu, Sheina, Kowalewski, &  
53 McCullough, 2002). Recently, we have reported the synthesis and morphological  
54 characterization of a carbohydrate-based block copolymer, poly(3-hexylthiophene)-*block*-  
55 peracetylated maltoheptaose (P3HT-*b*-AcMal<sub>7</sub>). We revealed that, via the thermal annealing of  
56 the copolymer thin film, the P3HT-*b*-AcMal<sub>7</sub> can self-organize into a periodic lamellar structure  
57 having a sub-10 nm scale *d*-spacing. This periodicity is one of the smallest domain sizes ever  
58 reported in block copolymers containing crystalline  $\pi$ -conjugated polymer blocks (Sakai-  
59 Otsuka et al., 2017). This distinct morphology could be attained by the huge chemical and steric  
60 disparity (high  $\chi$ ) between the synthetic P3HT block and the naturally-derived carbohydrate  
61 block. Furthermore, an enhanced thermal stability of the P3HT crystalline structure was  
62 observed when the P3HT segments were confined in the phase-separated P3HT-*b*-AcMal<sub>7</sub>  
63 lamellae (Sakai-Otsuka et al., 2020).

64 While our previous works have highlighted the great potential of the P3HT-*b*-AcMal<sub>7</sub> as a  
65 system with an ideal morphology for OPV securing a high stability of the P3HT crystalline  
66 structure, the two following questions are yet to be answered: (i) how the semiconducting  
67 domains are organized in the film and (ii) how the ordered D/A nanostructures can be achieved  
68 by taking advantage of self-organization of the P3HT-*b*-AcMal<sub>7</sub>. In this study, by addressing  
69 these questions, we aim at establishing a morphological control method best suited for our  
70 original P3HT-*b*-AcMal<sub>7</sub> system whilst providing the fine-tuned ideal D/A lamellar structures.

71 Controlling the morphology of photoactive layers remains a crucial challenge for  
72 performance enhancement of the OPVs. A perpendicularly-oriented periodic lamellar structure,  
73 in which electron donor and acceptor materials are alternately interpenetrating on the 10-nm  
74 length scale, has been recognized as an ideal geometry. This well-defined structure ensures (i)  
75 enlarged interface contact, (ii) optimal lateral domain size for exciton dissociation, (iii) the  
76 shortest charge transportation pathway in the vertical direction, and (iv) reduced charge trap  
77 sites (Coakley & McGehee, 2004; Shah & Ganesan, 2010). Although our previous study  
78 demonstrated the formation of the lamellar structures in the film, it was unclear how the  
79 semiconducting domains are organized with respect to the film surface.

80 Another issue is to achieve ordered D/A nanostructures by taking advantage of self-  
81 organization of the P3HT-*b*-AcMal<sub>7</sub>. For instance, in case of a blend of P3HT and [6,6]-phenyl  
82 C<sub>61</sub> butyric acid methyl ester (PC<sub>61</sub>BM), small PC<sub>61</sub>BM molecules are easily diffused over the  
83 photoactive layer due to the lack of physical or chemical connections to the P3HT matrix. This  
84 instability causes inhomogeneous macrophase segregations of the blends, undesired  
85 crystallization or aggregation of PC<sub>61</sub>BM, and eventually leads to the deterioration of device  
86 performance with long-term device operations or during post-annealing process. Several  
87 strategies have been implemented to localize fullerene-based *n*-type acceptors in a specific area  
88 of phase-separated block copolymer systems. Synthesizing D-A block copolymers consisting  
89 of a semiconducting donor polymer and another polymer bearing covalently attached acceptor

90 compounds is one of the promising approaches (Miyanishi, Zhang, Hashimoto, & Tajima, 2012;  
91 Miyanishi, Zhang, Tajima, & Hashimoto, 2010). Alternatively, non-covalent chemical  
92 interaction between acceptor materials and polymer blocks has also been exploited to  
93 immobilize the acceptors (Lin et al., 2012; Sary et al., 2010). Inspired by the latter approach, in  
94 this study, we designed a new fullerene derivative bearing AcMal<sub>7</sub> segment (AcMal<sub>7</sub>-C<sub>61</sub>) to  
95 immobilize the acceptor compounds in the AcMal<sub>7</sub> channel. We hypothesize that the AcMal<sub>7</sub>-  
96 C<sub>61</sub> would be excluded from P3HT domains during a post-thermal annealing process and  
97 predominately located within the phase-separated AcMal<sub>7</sub> domain owing to a total miscibility  
98 between the AcMal<sub>7</sub>-C<sub>61</sub> and AcMal<sub>7</sub> segments. Simultaneously, the AcMal<sub>7</sub>-C<sub>61</sub> is not  
99 expected to cause any microphase separation or crystallization of fullerenes in the AcMal<sub>7</sub>  
100 matrix because of a steric constraint of AcMal<sub>7</sub> moiety.

101 Here in, we present the synthesis of carbohydrate-based fullerene derivative AcMal<sub>7</sub>-C<sub>61</sub> and  
102 the reciprocal self-organization of the P3HT-*b*-AcMal<sub>7</sub>:AcMal<sub>7</sub>-C<sub>61</sub> blends. The chemical  
103 structure of the AcMal<sub>7</sub>-C<sub>61</sub> was fully characterized by NMR, FT-IR, and mass spectroscopy.  
104 **The** validity of the approach was confirmed by investigating the morphology of the P3HT-*b*-  
105 AcMal<sub>7</sub>:AcMal<sub>7</sub>-C<sub>61</sub> blends and crystalline structure of P3HT domains using transmission  
106 electron microscopy (TEM) and Wide-angle X-ray scattering (WAXS) analysis. In addition, an  
107 internal orientation of the self-assembled P3HT-*b*-AcMal<sub>7</sub> lamellar was investigated to gain  
108 further insight into the internal structure. TEM and grazing incidence small-angle X-ray  
109 scattering (GISAXS) measurements revealed that the P3HT-*b*-AcMal<sub>7</sub> tends to organize into  
110 perpendicularly-oriented lamellar structures relative to the film surface at the air/film boundary.

111

## 112 **2. Experimental Section**

### 113 *2.1. Materials*

114 [6,6]-Phenyl C<sub>61</sub> butyric acid methyl ester (PC<sub>61</sub>BM) was kindly gifted by PCAS (Longjumeau,  
115 France). Maltoheptaose was purchased from Nagase & Co., Ltd. (Japan). All other reagents

116 were purchased from Sigma-Aldrich and used as received without further purification unless  
117 otherwise specified. Reducing-end azide-functionalized peracetylated maltoheptaose  
118 (AcMal<sub>7</sub>-N<sub>3</sub>) and [6,6]-Phenyl C<sub>61</sub> butyric acid (PC<sub>61</sub>BA) were synthesized as previously  
119 reported (Hummelen et al., 1995; Sakai-Otsuka et al., 2017). Poly (3-hexylthiophene)-*b*-  
120 peracetylated maltoheptaose (P3HT-*b*-AcMal<sub>7</sub>) was synthesized via copper(I)-catalyzed 1,3-  
121 dipolar azide-alkyne cycloaddition (CuAAC) click reaction of alkyne-functionalized  
122 regioregular P3HT (alkyne-P3HT) with the AcMal<sub>7</sub>-N<sub>3</sub>. The alkyne-P3HT was prepared by  
123 post-functionalization modification of Br/H-terminated P3HT via Stille coupling between Br-  
124 terminated polymer end with ethynyltributylstannane. Details of the synthesis and  
125 characterizations were described in the supporting information.

126

## 127 2.2. Instruments

128 <sup>1</sup>H (400 MHz) and <sup>13</sup>C (100 MHz) NMR spectra were recorded using a Bruker Avance DRX  
129 400 MHz. FT-IR spectra were recorded using a Perkin-Elmer Spectrum RXI FT-IR  
130 Spectrometer. TEM and electron diffraction (ED) measurements were carried out using CM200  
131 Philips microscope (Thermo Fisher Scientific) operating at 200 kV equipped with a TVIPS  
132 F216 TemCam camera. Wide-angle X-ray scattering (WAXS) and Grazing incidence small-  
133 angle X-ray scattering (GISAXS) experiments were carried out on the BM02 beamline D2AM  
134 at the European Synchrotron Radiation Facility (ESRF, Grenoble, France). X-rays of 18 keV  
135 ( $\lambda = 0.6888 \text{ \AA}$ ) with a spot size of 100  $\mu\text{m}$  were used for WAXS. GISAXS was done with X-  
136 ray energy of 11 keV. Scattering patterns were recorded on two photon-counting pixel detectors  
137 (WOS and D5 from imXpad).

138

## 139 2.3. Synthesis of *N*-propargyl [6,6]-phenyl C<sub>61</sub> butyramido (alkyne-PC<sub>61</sub>BA)

140 In a dry 100 mL three-neck round-bottom flask equipped with a reflux condenser, PC<sub>61</sub>BA (200  
141 mg, 0.22 mmol, 1 equiv.) and thionyl chloride (4 mL) were introduced, and the mixture was

142 refluxed at 70 °C under an argon atmosphere until the FT-IR spectrum showed a complete  
143 disappearance of the peak at 1702 cm<sup>-1</sup> corresponding to the C=O stretching vibration of  
144 carboxylic acid group in the PC<sub>61</sub>BA. After the mixture was cooled to the room temperature,  
145 thionyl chloride was evaporated by vacuum pump. In another dry 50 mL flask, propargylamine  
146 (42.8 μL, 0.67 mmol, 3 equiv.), dry triethylamine (0.19 μL, 0.13 mmol, 6 equiv.) and THF (12  
147 mL) were added and the solution was degassed by bubbling with argon for 5 min and stirred at  
148 room temperature. The solution of the propargylamine was transferred to the reaction mixture  
149 via syringe under argon atmosphere. The mixture was stirred at room temperature for 4h until  
150 the FT-IR spectrum showed a complete disappearance of the peak at 1793 cm<sup>-1</sup> corresponding  
151 to the C=O stretching vibration of the carbonyl chloride group. The product was purified by  
152 precipitation in cold methanol and dried under reduced pressure to yield the *N*-propargyl [6,6]-  
153 phenyl C<sub>61</sub> butyramido (alkyne-PC<sub>61</sub>BAm) as a brown solid (88.5 mg, 43 %). <sup>1</sup>H-NMR (400  
154 MHz, THF-*d*<sub>8</sub>, δ): 8.01 (d, 2H, *o*-*H* aromatic), 7.53 (t, 2H, *m*-*H* aromatic), 7.44 (t, 1H, *p*-*H*  
155 aromatic), 7.34 (br, 1H, -*NH*-), 3.93 (m, 2H, -*CH*<sub>2</sub>-C≡CH), 2.97 (m, 2H, -*CH*<sub>2</sub>-CO-NH-), 2.53  
156 (1H, -C≡CH), 2.32 (t, 2H, Ph-C-*CH*<sub>2</sub>-), 2.16 (m, 2H, -*CH*<sub>2</sub>-*CH*<sub>2</sub>-CO-NH-); FT-IR (ATR): ν =  
157 1646 cm<sup>-1</sup> (C=O, butyramido); MALDI-TOF MS *m/z*: [M - H]<sup>-</sup> calcd for C<sub>74</sub>H<sub>14</sub>NO, 932.11;  
158 found, 932.93.

159

#### 160 2.4. Synthesis of fullerene-attached AcMal<sub>7</sub>(AcMal<sub>7</sub>-C<sub>61</sub>)

161 In a 250 ml flask, alkyne-PC<sub>61</sub>BAm (0.40 g, 0.43 mmol, 1 equiv.) and CuBr (91.6 mg, 0.64  
162 mmol, 1.5 equiv.) were dissolved in THF (60 mL), degassed by bubbling with argon for 5 min,  
163 and stirred at room temperature. In another 100 mL flask, AcMal<sub>7</sub>-N<sub>3</sub> (0.90 g, 0.43 mmol, 1  
164 equiv.) and PMDETA (134 μL, 0.64 mmol, 1.5 equiv.) were dissolved in THF (20 mL),  
165 degassed by bubbling with argon for 5 min, and stirred at room temperature. The solution of  
166 AcMal<sub>7</sub>-N<sub>3</sub> was transferred to the stirred solution of alkyne-PC<sub>61</sub>BAm via cannula under argon  
167 atmosphere. The reaction mixture was stirred at room temperature for 12h until the FT-IR

168 spectrum showed a complete disappearance of the signal corresponding to the azide group of  
169 AcMal<sub>7</sub>-N<sub>3</sub>. The reaction mixture was passed through a neutral alumina column to remove  
170 copper salt with a THF eluent. The crude product was purified by precipitation in cold methanol.  
171 The product was collected by centrifugation and dried under reduced pressure to give the  
172 AcMal<sub>7</sub>-C<sub>61</sub> as a brown solid (0.76 g, 58 %). MALDI-TOF MS *m/z*: [M + H]<sup>+</sup> calcd for  
173 C<sub>161</sub>H<sub>131</sub>N<sub>4</sub>O<sub>58</sub>, 3036.75; found, 3036.98.

174

### 175 2.5. Ultrathin section preparation for TEM

176 An about 10 μm-thick film was prepared by drop casting from a concentrated THF solution of  
177 P3HT-*b*-AcMal<sub>7</sub> onto a PTFE substrate. After complete evaporation of the solvent, the obtained  
178 thick film was annealed at 220 °C for 10 min under vacuum to induce the microphase  
179 separation. A thin gold layer with a thickness of about 20 nm was sputtered on the film to  
180 distinguish the top side from the bottom side of the film. The thick film was then soaked in  
181 absolute ethanol for 1 hour to dehydrate and embedded in an epoxy resin (Embed-812). The  
182 hardened resin block was set on an ultramicrotome with the film plane being orthogonal to the  
183 sectioning direction. Ultrathin sections with a thickness of less than 100 nm were obtained using  
184 a 35° diamond knife with a clearance angle of 6°, and mounted onto carbon-coated copper grid.

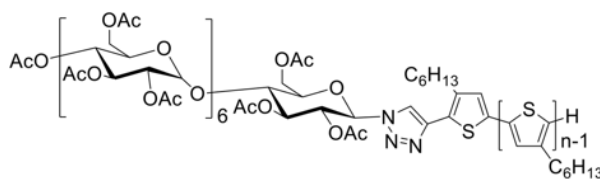
185

## 186 3. Results and Discussion

### 187 3.1. Lamellae Orientation of P3HT-*b*-AcMal<sub>7</sub>

188 The chemical structure and molecular properties of the P3HT-*b*-AcMal<sub>7</sub> used in this study  
189 are given in **Scheme 1** and **Table 1**, respectively. **Fig. 1a** shows a cross sectional TEM image  
190 of a thermally-annealed P3HT-*b*-AcMal<sub>7</sub> film in the vicinity of the interface of air (resin)/film  
191 surface. The film was prepared by a drop-casting on a PTFE-coated substrate with a thickness  
192 of *ca.* 10 μm. Interestingly, a lamellar structure oriented perpendicular to the surface was  
193 exclusively observed over more than 100 nm deep from the top surface while no preferential

194 orientation was observed at the bottom boundary (**Fig. S1**). This observation was further  
 195 confirmed by the GISAXS measurement. **Fig. 1b** shows a two-dimensional GISAXS pattern of  
 196 a thermally-annealed P3HT-*b*-AcMal<sub>7</sub> thin film with a film thickness of *ca.* 35 nm deposited  
 197 on a silicon substrate. Clear spots parallel to the substrate corresponding to a *d*-spacing of 12.6  
 198 nm were observed, indicating the perpendicular orientation of lamellae to the film surface.  
 199 Generally, if no treatment is applied, the perpendicular lamellar orientation of high- $\chi$  block  
 200 copolymers cannot be spontaneously obtained due to an inherent strong repulsive force between  
 201 the constituent blocks (Bates et al., 2012; Zhang et al., 2016). One of the two blocks that has a  
 202 more favorable interaction with the surface tends to align along the surface boundary to  
 203 minimize total interfacial energy, often resulting in the lamellar orientation parallel to the  
 204 surfaces. Unlike this trend, the P3HT-*b*-AcMal<sub>7</sub> manifests a perpendicularly-oriented lamellae  
 205 organization at the air boundary. While the reasons leading to this orientation are unknown for  
 206 the moment, the P3HT-*b*-AcMal<sub>7</sub> has a potential to realize a desirable perpendicular lamellar  
 207 organization across the entire film by tuning processing conditions or by using chemically  
 208 and/or topographically modified substrates.



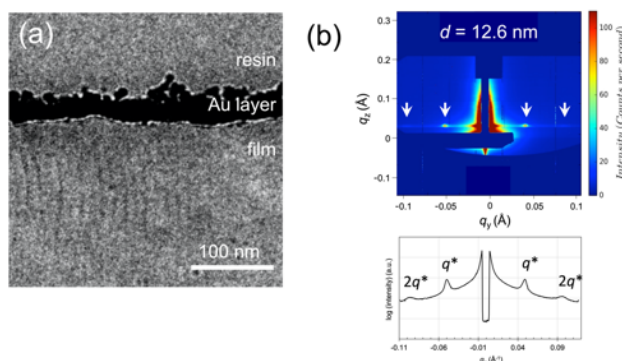
209  
210 **Scheme 1.** Chemical structure of P3HT-*b*-AcMal<sub>7</sub>.

211 **Table 1.** Molecular properties of the P3HT-*b*-AcMal<sub>7</sub> employed in this study  
212  
213

P3HT block					carbohydrate block	block copolymer	
$M_{n,SEC, P3HT}^{(a)}$ [g mol <sup>-1</sup> ]	$M_{w,SEC, P3HT}^{(a)}$ [g mol <sup>-1</sup> ]	$M_p, MALDI, P3HT^{(b)}$ [g mol <sup>-1</sup> ]	$D_{P3HT}^{(a)}$	% HT <sup>(c)</sup>	$M_{AcMal7}^{(d)}$ [g mol <sup>-1</sup> ]	$D_{total}^{(a)}$	$\phi_{P3HT}^{(e)}$
5670	6210	3682	1.07	> 95	2060	1.23	0.65

214 <sup>a)</sup>Number average molecular weight ( $M_n$ ), weight average molecular weight ( $M_w$ ), and  
 215 polydispersity ( $D$ ) determined by SEC in THF based on PS standards; <sup>b)</sup>molecular weight at the

216 peak maximum determined by MALDI-TOF MS; <sup>c</sup>HT-HT regioregularity determined by <sup>1</sup>H  
217 NMR; <sup>d</sup>molecular weight of carbohydrate block; <sup>e</sup>volume fraction of P3HT in copolymers  
218 calculated by using density values 1.16 g cm<sup>-3</sup> for P3HT and 1.20 g cm<sup>-3</sup> for AcMal<sub>7</sub>.  
219



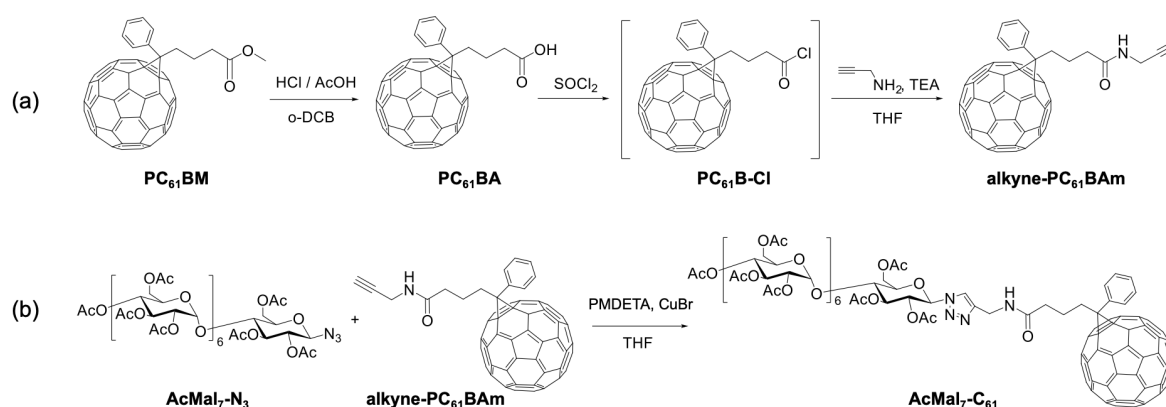
220

221 **Fig. 1.** (a) TEM image of the cross section of thermally annealed P3HT-*b*-AcMal<sub>7</sub> thick film in  
222 the vicinity of the film surface. (b) Two-dimensional GISAXS diffraction pattern of thermally  
223 annealed P3HT-*b*-AcMal<sub>7</sub> thin film.  
224

### 225 3.2. Synthesis of AcMal<sub>7</sub>-C<sub>61</sub>

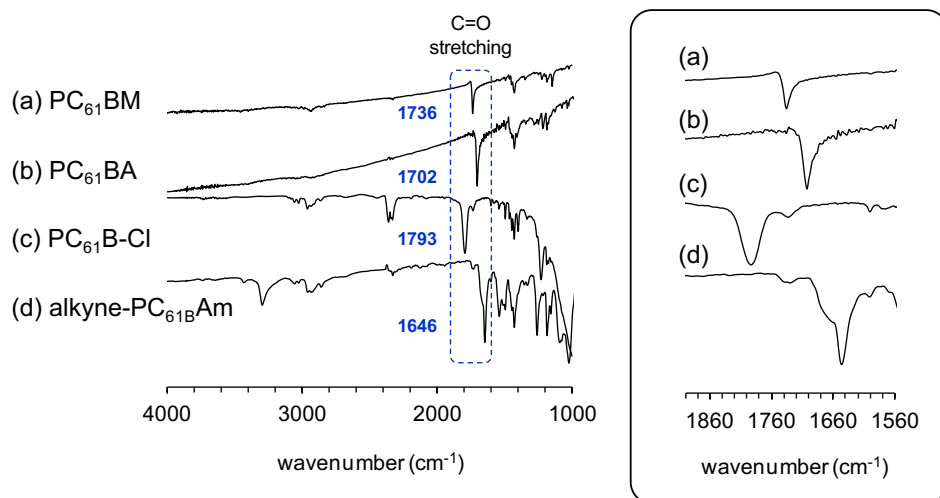
226 Fullerene-attached paracetylated maltoheptaose (AcMal<sub>7</sub>-C<sub>61</sub>) was synthesized as shown in  
227 **Scheme 2.** First, [6,6]-phenyl C<sub>61</sub> butyric acid (PC<sub>61</sub>BA) was prepared via hydrolysis of  
228 PC<sub>61</sub>BM following the literature procedure. (Hummelen et al., 1995) The PC<sub>61</sub>BA was then  
229 reacted with thionyl chloride (SOCl<sub>2</sub>) under reflux to afford reactive intermediate PC<sub>61</sub>B-Cl.  
230 Note that, carbon disulfide (CS<sub>2</sub>), which is known as one of the few good solvents for the  
231 PC<sub>61</sub>BA, is generally used for the reaction (Hummelen et al., 1995; Miyanishi et al., 2012).  
232 However, it was found from our experiment that the reaction proceeded well in the solvent-free  
233 condition. The PC<sub>61</sub>BA became soluble in the neat SOCl<sub>2</sub> over time and were completely  
234 converted to PC<sub>61</sub>B-Cl within six hours. Considering the boiling points of SOCl<sub>2</sub> ( $T_{b, SOCl_2} =$   
235 75 °C) and CS<sub>2</sub> ( $T_{b, CS_2} = 46$  °C), the absence of the CS<sub>2</sub> is more favorable to promote the  
236 reaction by heating near  $T_{b, SOCl_2}$ . Subsequently, the PC<sub>61</sub>B-Cl was reacted with propargylamine  
237 in the presence of dry trimethylamine to yield *N*-propargyl [6,6]-phenyl C<sub>61</sub> butyramido  
238 (alkyne-PC<sub>61</sub>BAm) as brown solid. The resulting product was soluble in tetrahydrofuran (THF)  
239 and hardly soluble in toluene, chloroform, and *o*-dichlorobenzene. The FT-IR spectrum of the

240 alkyne-PC<sub>61</sub>BAm showed the -C=O stretching band of amide group at 1646 cm<sup>-1</sup> but not the -  
 241 C=O stretching band of the carbonyl chloride at 1793 cm<sup>-1</sup>, indicating the complete conversion  
 242 of the PC<sub>61</sub>B-Cl to the corresponding amide (**Fig. 2**). <sup>1</sup>H NMR spectroscopy confirms the  
 243 presence of the ethynyl group at 2.53 ppm (**Fig. S2**) and the full substitution of the ethynyl  
 244 group by comparing the integrations of the signal at 2.53 ppm (signal a in **Fig. S2**) and proton  
 245 signals of phenyl ring (signal i-m in **Fig. S2**). The coupling of the alkyne-PC<sub>61</sub>BAm and  
 246 AcMal<sub>7</sub>-N<sub>3</sub> was performed via the CuAAC click reaction in THF. The crude product was  
 247 purified by passing through a neutral alumina column and precipitated into cold methanol to  
 248 afford AcMal<sub>7</sub>-C<sub>61</sub> as brown solid in 58 % yield. The resulting product was well soluble in THF,  
 249 chloroform, acetone, and *o*-dichlorobenzene and slightly soluble in toluene. <sup>1</sup>H NMR spectrum  
 250 of the product showed characteristic signals assignable to the protons of PC<sub>61</sub>BAm and AcMal<sub>7</sub>  
 251 (**Fig. S3**). The covalent attachment of the both moieties was confirmed by diffusion-ordered  
 252 spectroscopy (DOSY), showing a single diffusion coefficient with  $D = 3.8 \times 10^{-10} \text{ m}^2 \text{ s}^{-1}$  (**Fig.**  
 253 **3**). The absence of the characteristic IR band of the azide group at 2100 cm<sup>-1</sup> indicates the  
 254 completion of the reaction (**Fig. S4**). MALDI-TOF MS spectrometry provides further evidence  
 255 of the successful formation of the AcMal<sub>7</sub>-C<sub>61</sub>. The most intense peak at  $m/z$  3059.7 was  
 256 assignable to the target compound with sodium ion  $[M + \text{Na}]^+$  (**Fig. 4**).



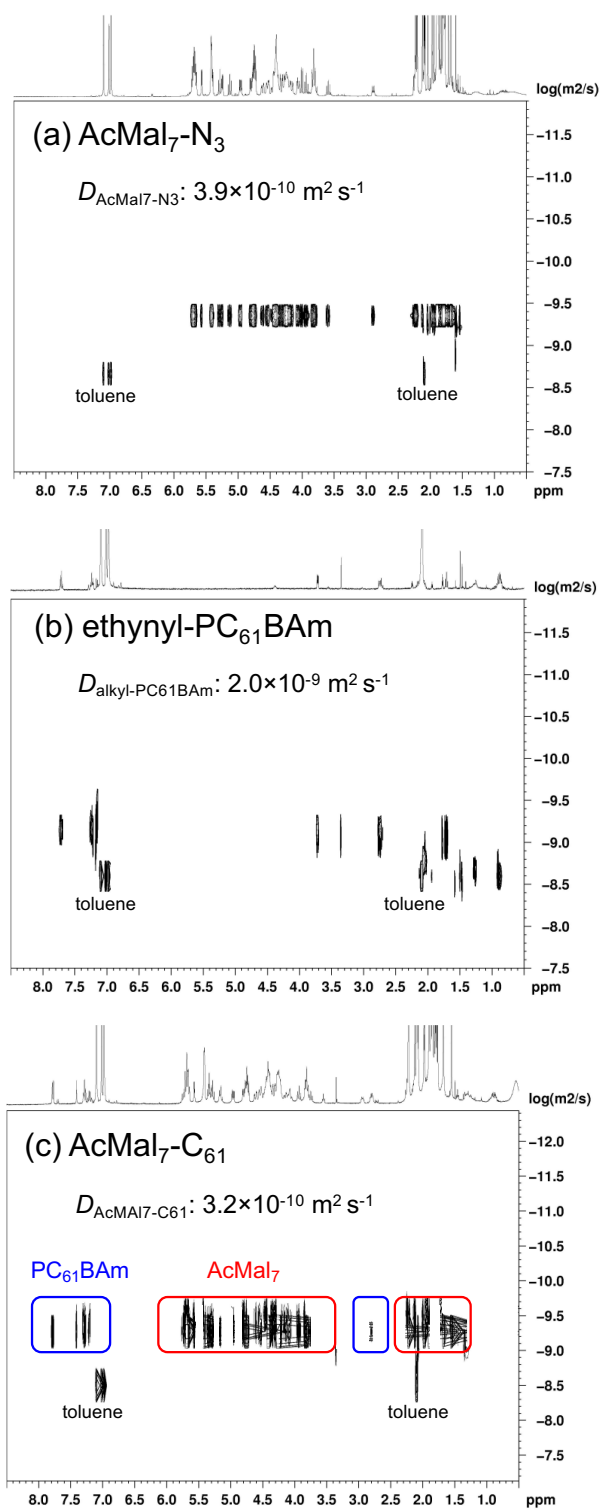
257  
 258 **Scheme 2.** Strategy used for the synthesis of AcMal<sub>7</sub>-C<sub>61</sub>: (a) Synthesis of alkyne-  
 259 functionalized fullerene (alkyne-PC<sub>61</sub>BAm) and (b) “Click” reaction of alkyne-PC<sub>61</sub>BAm with  
 260 azide endo-functionalized paracetylated maltoheptaose (AcMal<sub>7</sub>-N<sub>3</sub>).

261



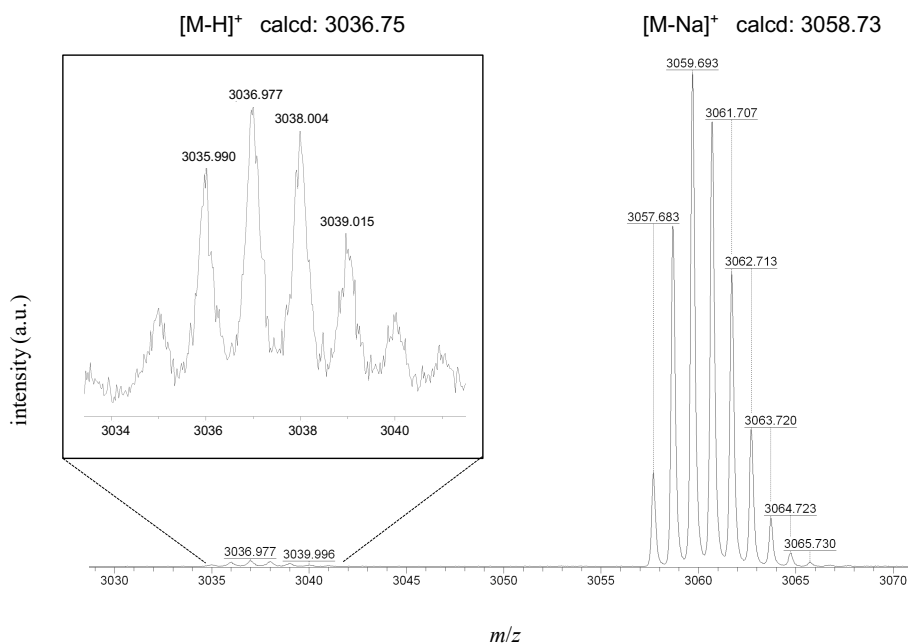
262

263 **Fig. 2.** FT-IR spectra of (a) PC<sub>61</sub>BM, (b) PC<sub>61</sub>BA, (c) PC<sub>61</sub>B-Cl, and (d) alkyne-PC<sub>61</sub>BAm.



264

265 **Fig. 3.** <sup>1</sup>H-DOSY spectra of (a) AcMal<sub>7</sub>-N<sub>3</sub>, (b) alkyne-PC<sub>61</sub>BAm, and (c) AcMal<sub>7</sub>-C<sub>61</sub> in  
 266 toluene-*d*<sub>8</sub>.



267

268

269

**Fig. 4.** MALDI-TOF MS spectrum of AcMal<sub>7</sub>-C<sub>61</sub> in positive mode.

### 270 3.3. Morphologies of P3HT-*b*-AcMal<sub>7</sub>:AcMal<sub>7</sub>-C<sub>61</sub> blends

271 The morphology of the blend films consisting of the P3HT-*b*-AcMal<sub>7</sub> and AcMal<sub>7</sub>-C<sub>61</sub> with

272 different donor(D):acceptor(A) composition ratio (w/w) was investigated by TEM. Note that

273 the D:A ratio was calculated based on the total weight of the donor segments (*i.e.* P3HT) in the

274 block copolymers with respect to that of acceptor moieties (*i.e.* fullerene) in the AcMal<sub>7</sub>-C<sub>61</sub>.

275 All films were annealed at 210 °C for 10 min prior to the TEM observations to induce the

276 microphase separation of the P3HT-*b*-AcMal<sub>7</sub>. The TEM image of a thermally-annealed

277 acceptor-free P3HT-*b*-AcMal<sub>7</sub> thin film showed a well-defined lamellar structure with a *d*-

278 spacing of *ca.* 12 nm as reported previously (**Fig. 5a**) (Sakai-Otsuka et al., 2020). At 1:0.1

279 loading ratio, the blend film exhibited a periodic stripe pattern identical to that of the P3HT-*b*-

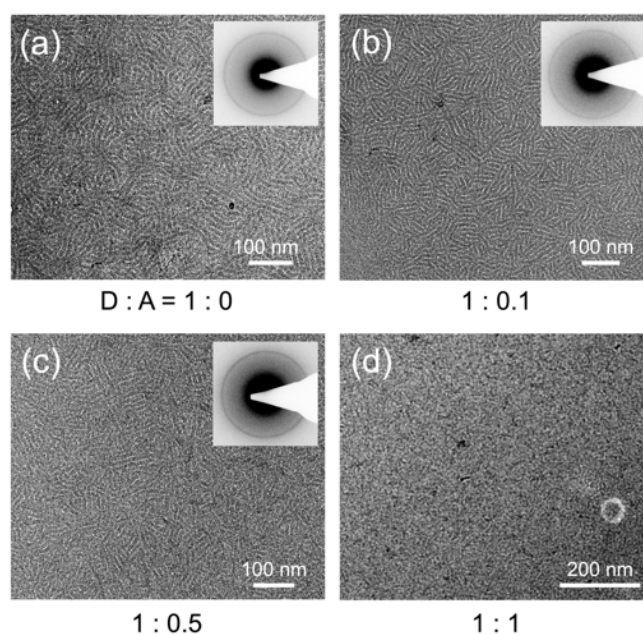
280 AcMal<sub>7</sub> film, indicating that the AcMal<sub>7</sub>-C<sub>61</sub> at low concentration disturbed neither P3HT

281 crystallization nor microphase separation of the P3HT-*b*-AcMal<sub>7</sub> (**Fig. 5b**). Electron diffraction

282 (ED) pattern inserted in **Fig. 5b** also supports this fact by showing a sharp 0 2 0 reflection

283 representing the  $\pi$ -stacking of the P3HT with a stacking period of *ca.* 3.8 Å. It is likely that the

284 AcMal<sub>7</sub>-C<sub>61</sub> molecules penetrate in the AcMal<sub>7</sub> domain of the phase-separated P3HT-*b*-AcMal<sub>7</sub>  
285 but are excluded from the P3HT domain without destroying the crystalline lamellar structure at  
286 this concentration. Upon increasing the D:A ratio up to 1:0.5, the diffraction pattern became  
287 less intense while the TEM image still showed the definite lamellar structures (**Fig. 5c**). At 1:1  
288 D:A ratio, no distinctive ordered structure was observed, indicating that this system reached  
289 order-disordered transition (**Fig. 5d**). Nevertheless, the blend films of P3HT-*b*-  
290 AcMal<sub>7</sub>:AcMal<sub>7</sub>-C<sub>61</sub> did not cause any crystallization of fullerene over the entire tested blend  
291 ratio range from 1:0.1 to 1:1 while a reference film of P3HT-*b*-AcMal<sub>7</sub>:PCBM at 1:1 induced  
292 many PCBM aggregations after thermal annealing at 210 °C for 10 min (**Fig. S5**).



293  
294 **Fig. 5.** TEM images of thermally annealed thin films of (a) P3HT-*b*-AcMal<sub>7</sub> and the blend of  
295 P3HT-*b*-AcMal<sub>7</sub> and AcMal<sub>7</sub>-C<sub>61</sub> with donor:acceptor ratio of (b) 1:0.1, (c) 1:0.5 and (d) 1:1  
296 (annealing condition: 210 °C for 10 min). Insets: electron diffraction patterns of the  
297 corresponding film.  
298

299 To assess the crystalline state of the P3HT and microscopic distribution of the AcMal<sub>7</sub>-C<sub>61</sub>,  
300 wide-angle X-ray scattering (WAXS) measurements were performed on the bulk samples of  
301 the P3HT-*b*-AcMal<sub>7</sub>:AcMal<sub>7</sub>-C<sub>61</sub> blends together with that of individual components (single  
302 P3HT-*b*-AcMal<sub>7</sub> and AcMal<sub>7</sub>-C<sub>61</sub>). For all samples, *h* 0 0 and 0 2 0 reflections, corresponding

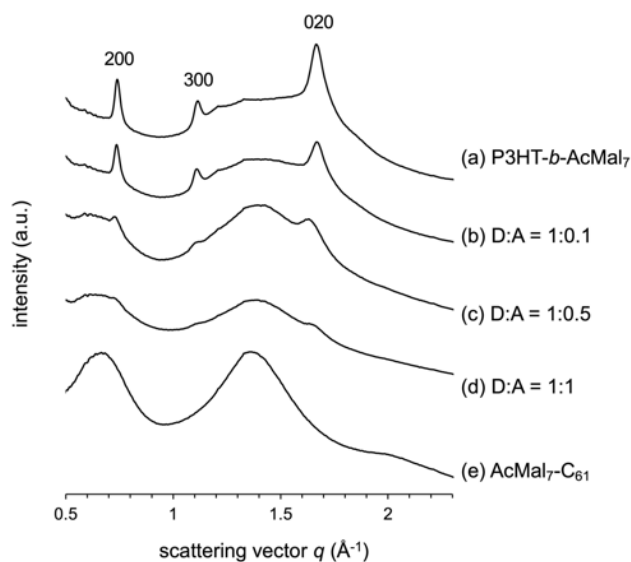
303 to the periodicity along the hexyl side chain direction and  $\pi$ -stacking periodicity, respectively,  
304 are visible while their intensities decrease with increasing acceptor content (**Fig. 6**). This means  
305 that the addition of the AcMal<sub>7</sub>-C<sub>61</sub> partially disrupts the crystallization of the P3HT segments.  
306 A broad amorphous scattering **originating** from a short-range ordering of molecular  
307 arrangement of the AcMal<sub>7</sub>-C<sub>61</sub> was observed in the WAXS profile of the AcMal<sub>7</sub>-C<sub>61</sub> (**Fig. 6e**)  
308 and might be present underneath the WAXS profiles of the blend samples.

309 If the addition of the AcMal<sub>7</sub>-C<sub>61</sub> does not affect the crystalline structure of the P3HT  
310 segments in the blend films, the scattering intensity should be expressed by a linear combination  
311 of two reference WAXS profiles of single substances (P3HT-*b*-AcMal<sub>7</sub> (**Fig. 6a**) and AcMal<sub>7</sub>-  
312 C<sub>61</sub> (**Fig. 6e**)) as illustrated in **Fig. S6**. For a weight fraction of P3HT-*b*-AcMal<sub>7</sub>,  $\alpha$  in the blend  
313 system, the expected scattering intensity,  $I_{cal}$  is given as:

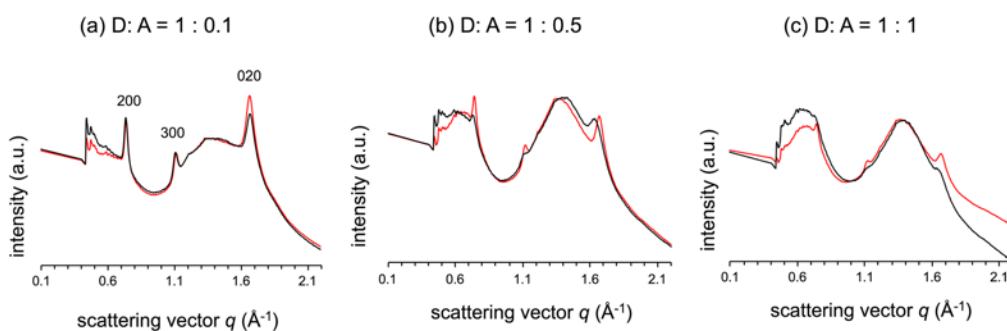
$$314 \quad I_{cal} = \alpha I_{donor} + (1 - \alpha) I_{acceptor}$$

315 where  $I_{donor}$  and  $I_{acceptor}$  are scattering intensities of the P3HT-*b*-AcMal<sub>7</sub> and AcMal<sub>7</sub>-C<sub>61</sub>,  
316 respectively. The comparison between experimental and calculated WAXS profiles **was**  
317 presented in **Fig. 7**. The calculated profiles were normalized with respect to integrated area of  
318 the corresponding WAXS profiles. At low 1:0.1 loading ratio, the calculated profile is almost  
319 identical with the experimental one except for a slightly higher intensity of the 0 2 0 reflection.  
320 At higher blend ratio, all peaks at  $h$  0 0 and 0 2 0 of the combined profile became less prominent  
321 compared to those of non-treated additive-free WAXS profile (**Fig. 6a**) as a consequence of the  
322 superposition of non-negligible amorphous halo of the AcMal<sub>7</sub>-C<sub>61</sub>. Although the  $h$  0 0 and 0 2  
323 0 peaks in the experimental data are broader, indicating the smaller crystallite size of P3HT, we  
324 can still recognize the crystalline nature of the P3HT segments. Hence, it is reasonable to  
325 assume that the AcMal<sub>7</sub>-C<sub>61</sub> molecules are exclusively incorporated in the phase-separated  
326 AcMal<sub>7</sub> nanodomains with limited deleterious effect on the initial lamellar morphology and  
327 crystalline structure of the P3HT segments. Otherwise, the closely-packed P3HT crystalline  
328 structure would not be maintained because of a bulkiness of the AcMal<sub>7</sub>-C<sub>61</sub> molecules. With

329 an adequate amount of the AcMal<sub>7</sub>-C<sub>61</sub>, the present P3HT-*b*-AcMal<sub>7</sub>:AcMal<sub>7</sub>-C<sub>61</sub> blend system  
 330 can provide a co-alternating D-A lamellar network at the exciton diffusion length scale, from  
 331 which we anticipate an improved photovoltaic performance despite the presence of the  
 332 insulating AcMal<sub>7</sub> segments in the blend.



333  
 334 **Figure 6.** WAXS profiles of the thermally-annealed bulk samples of the single component of  
 335 (a) P3HT-*b*-AcMal<sub>7</sub> and (e) AcMal<sub>7</sub>-C<sub>61</sub>, and thermally-annealed bulk samples of the blend of  
 336 P3HT-*b*-AcMal<sub>7</sub> and AcMal<sub>7</sub>-C<sub>61</sub> with a donor:acceptor ratio of (b) 1:0.1, (c) 1:0.5 and (d) 1:1  
 337 (annealing condition : 210 °C for 10 min).  
 338



339  
 340 **Fig. 7.** Comparison between experimental WAXS profiles (black) and simulated profiles (red)  
 341 for the blends of P3HT-*b*-AcMal<sub>7</sub> and AcMal<sub>7</sub>-C<sub>61</sub> with donor:acceptor ratio of (a) 1:0.1, (b)  
 342 1:0.5 and (c) 1:1.  
 343

#### 344 4. Conclusion

345 We have demonstrated the well-defined D/A lamellar structures through a reciprocal self-  
346 organization of carbohydrate-*b*-P3HT block copolymer and a strategically designed  
347 carbohydrate-based fullerene derivative AcMal<sub>7</sub>-C<sub>61</sub>. The AcMal<sub>7</sub>-C<sub>61</sub> was synthesized via  
348 CuAAC “click” reaction of the alkyne-functionalized fullerene and azido-functionalized  
349 AcMal<sub>7</sub>. The synthesized acceptor compound showed a good solubility in various organic  
350 solvents including THF, chloroform, acetone, and *o*-dichlorobenzene, which is advantageous  
351 for solution-based film fabrications. As expected from the different compatibility of AcMal<sub>7</sub>-  
352 C<sub>61</sub> to P3HT and AcMal<sub>7</sub>, a morphological investigation of the blend system proved that the  
353 AcMal<sub>7</sub>-C<sub>61</sub> molecules are localized in the phase-separated AcMal<sub>7</sub> nanodomains upon  
354 annealing without causing the formation of fullerene crystals. The crystallinity of P3HT and  
355 well-defined lamellar morphology that were observed in the single P3HT-*b*-AcMal<sub>7</sub> film were  
356 retained up to 1:0.5 (D:A) blending ratio. This result indicates that the addition of newly  
357 designed AcMal<sub>7</sub>-C<sub>61</sub> to the highly-segregated P3HT-*b*-AcMal<sub>7</sub> block copolymer system could  
358 be a valuable approach to realize a conceptionally optimal D/A lamellar structures with sub-10  
359 nm domain features, which ensures the effective exciton dissociation at the D/A interface.  
360 Additionally, cross-sectional TEM observation and GISAXS measurement revealed that the  
361 P3HT-*b*-AcMal<sub>7</sub> tends to spontaneously organize into perpendicularly-oriented lamellar  
362 structures relative to the film surface at the air/film interface while at the bottom interface the  
363 domain orientation depends on the nature of the substrate. This inherent nature of our high- $\chi$   
364 block copolymer system would be industrially beneficial since no additional treatment, such as  
365 top-coat application, is required to control lamellar orientation at the top interface. The tuning  
366 of the microphase separation and investigation of charge carrier mobility of the ordered  
367 photoactive blend films are topics of future study.

368

369 **Acknowledgements**

370 R.B. acknowledges partial financial support from “SweetMemory” International France-  
371 Taiwan ANR project [#ANR-14-CE08-0021], Institute Carnot PolyNat ANR [#CARN-025-01]  
372 and the European Union’s Seventh Framework Program [FP7/2007-2013] under grant  
373 agreement n° 603519. This work was financially supported by the JSPS Grant-in-Aid for  
374 Scientific Research (B) [19H02769, T. S.], the Photoexcitonix Project (Hokkaido University,  
375 T. S.), and Creative Research Institute (CRIS, Hokkaido University, T. S.). The WOS was  
376 funded by the ANR under the "Investissements d'avenir" program [ANR-11-EQPX-0010]. R.B.  
377 would like to gratefully thank the CNRS and Grenoble Alpes University for partial financial  
378 support in this project, the Advanced Research Center for Green Materials Science and  
379 Technology, National Taiwan University (NTU) and Hokkaido University (Laboratory of  
380 Polymer Chemistry, Faculty of Engineering) for exchange students and fruitful collaboration.

381

382 **Supporting Information**

383 Supporting Information is available at: XXXXXX.

384

385 **References**

- 386 Bates, C. M., Seshimo, T., Maher, M. J., Durand, W. J., Cushen, J. D., Dean, L. M., Willson,  
387 C. G. (2012). Polarity-Switching Top Coats Enable Orientation of Sub-10-nm Block  
388 Copolymer Domains. *Science*, 338(6108), 775–779.  
389 <https://doi.org/10.1126/science.1226046>
- 390 Boudouris, B. W., Frisbie, C. D., & Hillmyer, M. A. (2008). Nanoporous Poly(3-  
391 alkylthiophene) Thin Films Generated from Block Copolymer Templates.  
392 *Macromolecules*, 41(1), 67–75. <https://doi.org/10.1021/ma071626d>
- 393 Coakley, K. M., & McGehee, M. D. (2004). Conjugated Polymer Photovoltaic Cells. *Chemistry*  
394 *of Materials*, 16(23), 4533–4542. <https://doi.org/10.1021/cm049654n>
- 395 Dou, L., You, J., Hong, Z., Xu, Z., Li, G., Street, R. A., & Yang, Y. (2013). 25th Anniversary  
396 Article: A Decade of Organic/Polymeric Photovoltaic Research. *Advanced Materials*,  
397 25(46), 6642–6671. <https://doi.org/10.1002/adma.201302563>
- 398 Hummelen, J. C., Knight, B. W., LePeq, F., Wudl, F., Yao, J., & Wilkins, C. L. (1995).  
399 Preparation and Characterization of Fulleroid and Methanofullerene Derivatives. *The*  
400 *Journal of Organic Chemistry*, 60(3), 532–538. <https://doi.org/10.1021/jo00108a012>
- 401 Iovu, M. C., Zhang, R., Cooper, J. R., Smilgies, D. M., Javier, A. E., Sheina, E. E., Kowalewski,  
402 T., McCullough, R. D. (2007). Conducting Block Copolymers of Regioregular Poly(3-

403 hexylthiophene) and Poly(methacrylates): Electronic Materials with Variable  
404 Conductivities and Degrees of Interfibrillar Order. *Macromolecular Rapid*  
405 *Communications*, 28(17), 1816–1824. <https://doi.org/10.1002/marc.200700401>

406 Lee, Y., & Gomez, E. D. (2015). Challenges and Opportunities in the Development of  
407 Conjugated Block Copolymers for Photovoltaics. *Macromolecules*, 48(20), 7385–7395.  
408 <https://doi.org/10.1021/acs.macromol.5b00112>

409 Lin, Y., Lim, J. A., Wei, Q., Mannsfeld, S. C. B., Briseno, A. L., & Watkins, J. J. (2012).  
410 Cooperative Assembly of Hydrogen-Bonded Diblock Copolythiophene/Fullerene Blends  
411 for Photovoltaic Devices with Well-Defined Morphologies and Enhanced Stability.  
412 *Chemistry of Materials*, 24(3), 622–632. <https://doi.org/10.1021/cm203706h>

413 Liu, J., Sheina, E., Kowalewski, T., & McCullough, R. D. (2002). Tuning the Electrical  
414 Conductivity and Self-Assembly of Regioregular Polythiophene by Block  
415 Copolymerization: Nanowire Morphologies in New Di- and Triblock Copolymers We  
416 gratefully acknowledge support from the NSF (CHE-9807707). *Angewandte Chemie*  
417 *International Edition*, 41(2), 329. [https://doi.org/10.1002/1521-3773\(20020118\)41:2<329::AID-ANIE329>3.0.CO;2-M](https://doi.org/10.1002/1521-3773(20020118)41:2<329::AID-ANIE329>3.0.CO;2-M)

419 Miyanishi, S., Zhang, Y., Hashimoto, K., & Tajima, K. (2012). Controlled Synthesis of  
420 Fullerene-Attached Poly(3-alkylthiophene)-Based Copolymers for Rational  
421 Morphological Design in Polymer Photovoltaic Devices. *Macromolecules*, 45(16), 6424–  
422 6437. <https://doi.org/10.1021/ma300376m>

423 Miyanishi, S., Zhang, Y., Tajima, K., & Hashimoto, K. (2010). Fullerene attached all-  
424 semiconducting diblock copolymers for stable single-component polymer solar cells.  
425 *Chemical Communications*, 46(36), 6723. <https://doi.org/10.1039/c0cc01819h>

426 Sakai-Otsuka, Y., Nishiyama, Y., Putaux, J.-L., Brinkmann, M., Satoh, T., Chen, W.-C., &  
427 Borsali, R. (2020). Competing Molecular Packing of Blocks in a Lamella-Forming  
428 Carbohydrate- block -poly(3-hexylthiophene) Copolymer. *Macromolecules*, in press.  
429 <https://doi.org/10.1021/acs.macromol.0c01801>

430 Sakai-Otsuka, Y., Zaioncz, S., Otsuka, I., Halila, S., Rannou, P., & Borsali, R. (2017). Self-  
431 Assembly of Carbohydrate- block -Poly(3-hexylthiophene) Diblock Copolymers into Sub-  
432 10 nm Scale Lamellar Structures. *Macromolecules*, 50(8), 3365–3376.  
433 <https://doi.org/10.1021/acs.macromol.7b00118>

434 Sary, N., Richard, F., Brochon, C., Leclerc, N., Lévêque, P., Audinot, J.-N., Berson, S., Heiser,  
435 T., Hadziioannou, G., Mezzenga, R. (2010). A New Supramolecular Route for Using Rod-  
436 Coil Block Copolymers in Photovoltaic Applications. *Advanced Materials*, 22(6), 763–  
437 768. <https://doi.org/10.1002/adma.200902645>

438 Segalman, R. A., McCulloch, B., Kirmayer, S., & Urban, J. J. (2009). Block Copolymers for  
439 Organic Optoelectronics. *Macromolecules*, 42(23), 9205–9216.  
440 <https://doi.org/10.1021/ma901350w>

441 Shah, M., & Ganesan, V. (2010). Correlations between Morphologies and Photovoltaic  
442 Properties of Rod–Coil Block Copolymers. *Macromolecules*, 43(1), 543–552.  
443 <https://doi.org/10.1021/ma9020467>

444 Yu, G., Gao, J., Hummelen, J. C., Wudl, F., & Heeger, A. J. (1995). Polymer photovoltaic cells:  
445 Enhanced efficiencies via a network of internal donor-acceptor heterojunctions. *Science*,  
446 270(5243), 1789. <https://doi.org/10.1126/science.270.5243.1789>

447 Zhang, J., Clark, M. B., Wu, C., Li, M., Trefonas, P., & Hustad, P. D. (2016). Orientation  
448 Control in Thin Films of a High- $\chi$  Block Copolymer with a Surface Active Embedded  
449 Neutral Layer. *Nano Letters*, 16(1), 728–735.  
450 <https://doi.org/10.1021/acs.nanolett.5b04602>

451  
452

453 A carbohydrate-based fullerene derivative is designed, synthesized and applied to a lamellar-  
454 forming high- $\chi$  block copolymer system to realize an ordered donor/acceptor (D/A) network.  
455 A well-defined D/A lamellar structure of the blend with sub-10 nm domain features, which  
456 ensures the effective exciton dissociation at the D/A interface, is achieved upon thermal  
457 annealing.  
458  
459